Introduction

In wave-equation migration, the imaging procedure consists of two steps: wavefield extrapolation of each shot source and receiver wavefields and the application of an imaging condition (Claerbout, 1985). The first step is linear but also time consuming and computationally intensive, especially if costly time-domain finite difference schemes are used for modeling wave propagation; the second step is relatively cheap from the computational point of view, but nonlinear. The high computational cost of wave-equation migration is balanced by the ability of dealing with multipathing, steep dips, and in the case of reverse-time migration, overturning and prismatic waves (Gray et al., 2001).

Shot-encoding migration was developed for reducing the computational cost of wave-equation migration. Morton and Ober (1998) and Romero et al. (2000) analyze the effects of simultaneously migrating a number of shots, linearly combined after the application of either random or linear delays, in particular they explore the crosstalk between different shot wavefields. Sourbaras (2006) presents a different strategy that exploits a unitary transformation for combining the original shots and for avoiding crosstalk.

In this abstract, we present an analysis of shot-encoding schemes that are suitable for reverse-time migration, namely random-shot encoding (R-SEM) (Romero et al., 2000) and plane-wave migration (linear shot-encoding, L-SEM) (Zhang et al., 2005). We analyze the behavior of these two methods with respect to crosstalk artifacts and spatial resolution in the final image. An optimal encoding reduces the crosstalk, while maintaining high image resolution. L-SEM emphasizes low crosstalk, while R-SEM emphasizes high spatial resolution. Here, we discuss a hybrid encoding scheme that combines the attributes of L-SEM and R-SEM. Tests on the synthetic Sigsbee model show that the new method is more effective than both L-SEM and R-SEM in achieving the mentioned imaging goals.

Mixed shot-encoding migration

Shot-encoding migration consists in imaging a linear superposition of source and receiver wavefields $s_k(\mathbf{x},t)$ and $r_k(\mathbf{x},t)$, corresponding to all the acquired shots. The new synthetic wavefields are then $S(\mathbf{x},t,\theta)=\sum_k s_k(\mathbf{x},t-f(\mathbf{x}_k,\theta))$ and $R(\mathbf{x},t,\theta)=\sum_l r_l(\mathbf{x},t-f(\mathbf{x}_l,\theta))$, where $f(\mathbf{x}_k,\theta)$ represents the delay applied to the k-th shot wavefields as a function of the shot position $\mathbf{x}_k$ and the parameter θ. The image is given by the time crosscorrelation of the new synthetic wavefields followed by stacking over the parameter θ, $I(\mathbf{x})=\sum_\theta\sum_t S(\mathbf{x},t,\theta)R(\mathbf{x},t,\theta)$. Substituting the expressions for $S(\mathbf{x},t,\theta)$ and $R(\mathbf{x},t,\theta)$ and transforming into the Fourier domain, we obtain the following expression for the shot-encoded image:

$$I(\mathbf{x})=\sum_\omega\sum_k\sum_l \tilde{s}_k(\mathbf{x},\omega)\tilde{r}_l^*(\mathbf{x},\omega)\sum_\theta e^{i\omega[f(\mathbf{x}_l,\theta)-f(\mathbf{x}_k,\theta)]}. \quad (1)$$

An encoding scheme is considered equivalent to shot-record migration if the condition

$$\sum_\theta e^{i\omega[f(\mathbf{x}_l,\theta)-f(\mathbf{x}_k,\theta)]}\approx\delta_{kl} \quad (2)$$

is satisfied, where δ_{kl} is the Kronecker symbol. Linear shot-encoding (L-SEM) satisfies Equation 2 given that a large number of θ values is used (F. Liu and Stolt, 2006), although the number of plane waves we need depends on the complexity of the model. With an insufficient number of plane-wave components, we are not able to completely cancel the crosstalk and we obtain a poorly resolved image.

Random shot-encoding (R-SEM) (Morton and Ober, 1998) combines all the shots with random delays in order to produce randomly distributed artifacts in the image. The artifacts stack out by summing up the images obtained from different realization of random encoding delays. R-SEM images a large number of the spatial spectrum and attenuation of the artifacts is proportional to the number of synthetic experiments migrated (Romero et al., 2000). Figures 1(a) and 1(b) show the main features of L-SEM and R-SEM. The first presents a low noise level because of the convergence of the crosstalk term toward the identity but it is limited in spatial bandwidth. On the contrary, the second recovers the maximum spatial bandwidth but introduces strong artifacts.

Mixed shot-encoding migration (M-SEM) consists in dithering an initial plane wave with a random perturbation: in this case, the delay function takes the form $f(\mathbf{x}_k,\theta)=\frac{\sin(\alpha\theta)}{v}(\mathbf{x}_k-\mathbf{x}_0)+t_k^\theta$; the first term

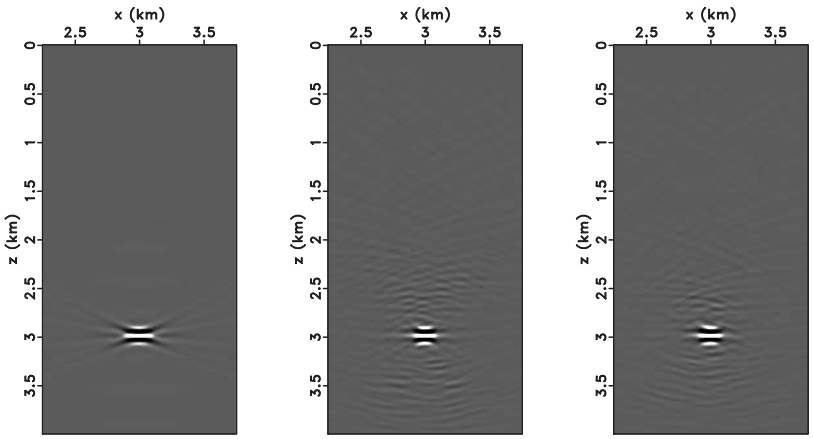

(a) (b) (c)

Figure 1: Point scatterer in a constant medium: (a) L-SEM, (b) R-SEM, and (c) M-SEM. For L-SEM, the limitation in spatial components results in a observable horizontal spreading. R-SEM produces a sharper image but creates artifacts; M-SEM provides a full-bandwidth image and controls the crosstalk.

represents the linear delay of L-SEM, where v is the surface velocity, $\alpha\theta$ the take-off angle of a specific plane wave and $\mathbf{x}_0$ is a reference point. The second term is the superimposed random perturbation and t_k^θ is a random variable. The behavior of M-SEM can be inferred from the coupling term in Equation 1. If we separate the terms for $k = l$ and highlight the interference between different shots, we obtain

$$W_{mixed}(\mathbf{x}_l, \mathbf{x}_k) = M\delta_{kl} + \sum_{\theta, k \neq l} e^{i\omega\left[\left(\frac{\sin(\alpha\theta)}{v} + \frac{\Delta t_{kl}^\theta}{\Delta \mathbf{x}_{kl}}\right)\Delta \mathbf{x}_{kl}\right]}. \tag{3}$$

where M is the number of synthetic experiments, $\Delta\mathbf{x}_{kl} = \mathbf{x}_l - \mathbf{x}_k$ and $\Delta t_{kl}^\theta = t_l^\theta - t_k^\theta$.

The ratio $\frac{\Delta t_{kl}^\theta}{\Delta \mathbf{x}_{kl}}$ has dimensions of ray parameter (s/m) and can be considered a perturbation of the ray parameter $\frac{\sin(\alpha\theta)}{v}$. The perturbation varies spatially, since it depends on $\Delta\mathbf{x}_{kl}$; the non-stationary nature of the ratio $\frac{\Delta t_{kl}^\theta}{\Delta \mathbf{x}_{kl}}$ allows us to gain spatial resolution with respect to standard L-SEM, since a greater number of "equivalent" spatial components $p_\theta^{eq} = \frac{\sin(\alpha\theta)}{v} + \frac{\Delta t_{kl}^\theta}{\Delta \mathbf{x}_{kl}}$ is imaged, but it also introduces a disturbance in the convergence of the crosstalk matrix toward the identity operator, i.e., random-like artifacts in the final image.

Let us analyze two extreme case; if $\Delta\mathbf{x}_{kl} \to 0$, then $p_\theta^{eq} \to \frac{\Delta t_{kl}^\theta}{\Delta \mathbf{x}_{kl}}$; on the other hand, if $\Delta\mathbf{x}_{kl} \to \infty$, then $p_\theta^{eq} \to \frac{\sin(\alpha\theta)}{v}$. Mixed shot-encoding behaves like R-SEM when we consider neighboring shots ("small" $\Delta\mathbf{x}_{kl}$), and tends toward L-SEM when we look at the effects on a particular shot from more distant ones ("large" $\Delta\mathbf{x}_{kl}$). This different behavior is the reason for the increase in the spatial resolution (with respect to L-SEM) and decrease in crosstalk (with respect to R-SEM) that M-SEM is able to achieve (see Figure 1(c)). Figures 2(a)-2(c) highlight the main features described above. The M-SEM coupling matrix converges faster to the identity than both the L-SEM and R-SEM ones; moreover, the control over the out-of-diagonal terms reduces the crosstalk in the image.

Sigsbee synthetic example

We apply the methodology described in the preceding section to the Sigsbee dataset and compared conventional shot-record migration (SRM) with L-SEM, R-SEM and M-SEM. The SRM result uses 50 out of the 500 shots of the complete survey. The shot-encoding results involve 50 synthetic experiments; the maximum delay is the same for the different encoding strategies and equal to 4s in order to ensure identical computational cost for the different techniques. The computational cost is 10% of the complete SRM image. Figures 3(a)-3(d) show a detail of the migrated image above the salt body; SRM shows

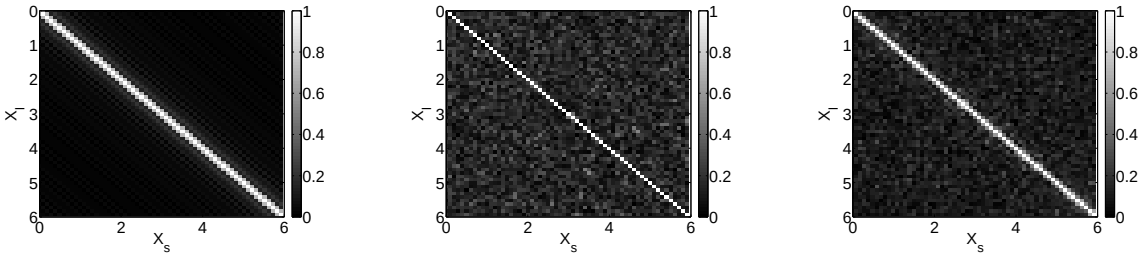

(a) (b) (c)

Figure 2: Absolute value of coupling term in Equation 1 for 30 synthetic experiments; (a) L-SEM, (b) R-SEM, and (c) M-SEM. x_s and x_l are shot positions, the out-of-diagonal terms represent the interference between different shots.

residual diffraction in proximity of the salt boundary and in the canyon because of shot undersampling. L-SEM recovers the nearly horizontal events, but blurs the top of the salt and does not image the flank in the canyon because of the limitation in the range of plane-wave components imaged. R-SEM supplies a full spatial bandwidth image but also introduces artifacts; M-SEM appreciably reduces the crosstalk, while imaging most of the spatial components.

Below the salt body (Figures 4(a)-4(d)), we observe stronger residual diffractions in SRM image (at $z = 5$km) because of shot undersampling; L-SEM is not able to image the faults, because of both illumination and distortion by the salt body, but supplies a clear image of the sediments; R-SEM recovers the full spatial information, particularly faults and point scatterers, but the poor illumination causes the crosstalk to overwhelm the signal and the image is hard to interpret. M-SEM achieves a good compromise between crosstalk and spatial resolution, being able to image faults (at $x = 10$km) and point scatterers (at $z = 5.2$km).

Conclusions

We analyze linear and random shot-encoding migration from the point of view of the behavior with respect to crosstalk noise and spatial bandwidth. We recognize complementary features and design a hybrid encoding scheme that is more robust against crosstalk artifacts preserving the spatial detail in the final image. Our strategy converges faster than both linear and random shot-encoding to the shot-profile migration result, thus reducing the overall cost of imaging for specified bandwidth and signal-to-noise ratio in the migrated image.

Acknowledgments

We would like to acknowledge the financial support provided by a research grant from Eni E&P, and stimulating technical discussions with Clara Andreoletti and Nicola Bienati.

REFERENCES

Claerbout, J. F., 1985, Imaging the earth's interior: Blackwell Publishing.

F. Liu, D. W. Hanson, N. D. W. R. S. D., and R. H. Stolt, 2006, Toward a unified analysis for source plane wave migration: Geophysics, **71**, S129–S139.

Gray, S. H., J. Etgen, J. Dellinger, and D. Whitmore, 2001, Seismic migration problems and solutions: Geophysics, **66**, 1622–1640.

Morton, S. A., and C. C. Ober, 1998, Faster shot-record migrations using phase encoding: 68th Ann. Internat. Mtg, Soc. of Expl. Geophys., 1131–1134.

Romero, L. A., D. C. Ghiglia, C. C. Ober, and S. A. Morton, 2000, Phase encoding of shot records in prestack migration: Geophysics, **65**, 426–436.

Sourbaras, R., 2006, Modulated-shot migration: 76th Ann. Internat. Mtg., Soc. of Expl. Geophys., 2430–2433.

Zhang, Y., J. Sun, C.Notfors, S. H. Gray, L. Chernis, and J. Young, 2005, Delayed-shot 3d depth migration: Geophysics, **70**, E21–E28.

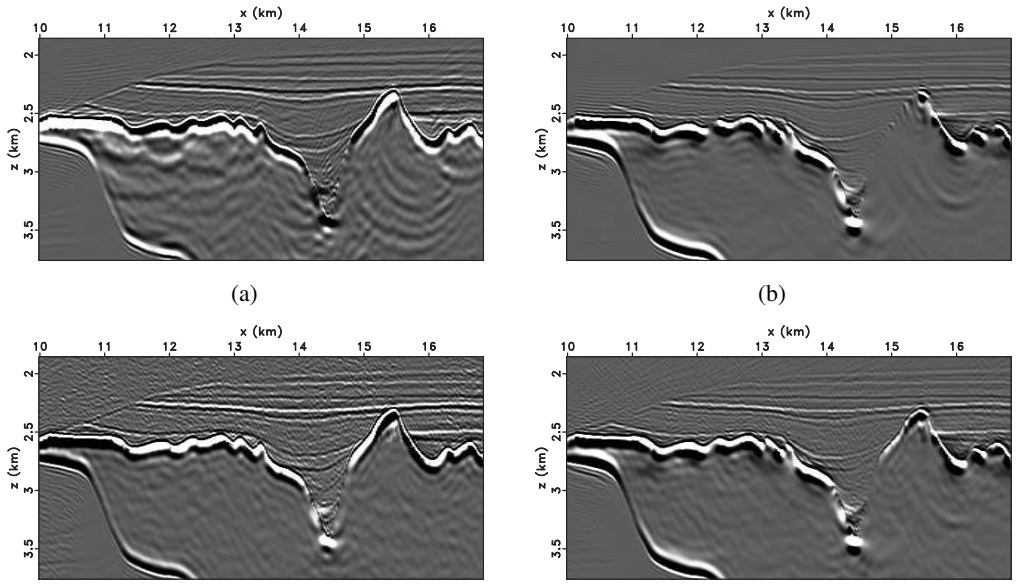

Figure 3: Image detail above the Sigsbee2A salt body: (a) SRM, (b) L-SEM, (c) R-SEM, and (d) M-SEM. Observe the residual diffractions in the SRM image due to the undersampling of the shot dimension. L-SEM is able to recover the nearly horizontal events, but the top of salt is smoothed out and the steep flanks of the salt canyon are not well imaged. R-SEM introduces random-like noise but images correctly the structures and the rugose top of the salt. M-SEM reduces the crosstalk, images correctly the nearly horizontal events and obtains a better image of the top of the salt.

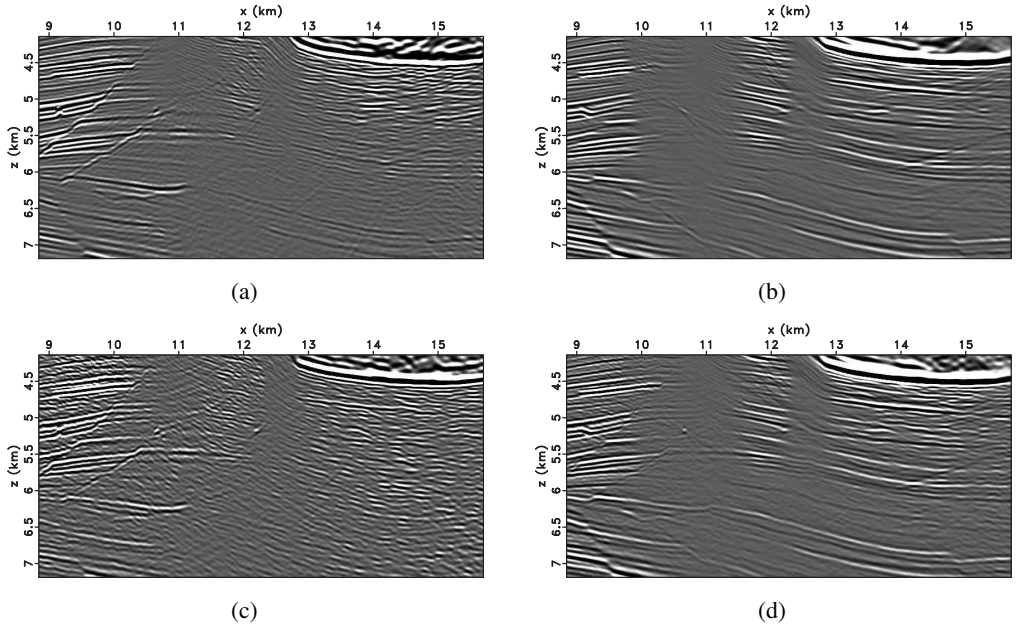

Figure 4: Image detail below the Sigsbee2A salt body: (a) SRM, (b) L-SEM, (c) R-SEM, and (d) M-SEM. The undersampling of the shot dimension is particularly important below the salt bodies and results in residual diffraction events that distort the image. L-SEM images correctly nearly horizontal events but loses the fault information and the point diffractors. R-SEM reconstructs the complete spatial information but introduces crosstalk noise below the salt, where illumination is poor. M-SEM provides a clearer image, with respect to R-SEM, better images the faults and the point diffractors, compared with L-SEM, and achieves an interpretable image below the salt, in contrast to SRM, in which the residual diffractions mask the sediments.